Design and Fabrication of a Delta Wing Micro Aerial Vehicle

SEPIDEH AFSHAR, AGHIL YOUSEFI-KOMA, HOSSEIN SHAHI,
DONYA MOHAMMADSHAHI, HESAM MALEKI

***Abstract*—** Design and fabrication of a bodyless MAV is presented in this paper. Bodyless MAVs take advantage of more lift and less drag. A triangular wing is chosen to this end and two models are fabricated to investigate winglet effect in aerodynamic properties, especially roll and yaw stability. Results show that this wing provides better results than conventional models. Moreover, the model proves good maneuverability characteristics. It is also shown, in the designed MAV, lack of winglets results in stability reduction.

***Keywords*—** Delta wing - Bodyless – Micro aerial vehicle - Aerodynamic analysis.

I. INTRODUCTION

Unmanned Aerial Vehicle (UAV) development was inspired by the evaluation of piloted airplanes. Interest in the design and development of small UAVs began for more than 25 years ago [1]. Although the definition of small UAVs is arbitrary, vehicles with length less than 6m and mass less than 25 kg are usually considered to be in this category. Designing of aircraft which are as small as possible attracts a serious effort to make use in special and limited-duration military and civil mission. These aircraft are called Micro Aerial Vehicle (MAV).

MAVs are of interest because electronic surveillance and detection sensor equipments can now be miniaturized. And so leads to developed aircraft with a 15-cm maximum dimension that have a mass of less than 90gr. The payload mass vs. wing span for MAVs and UAVs is presented in fig. 1.

The technical research on MAVs, started about 12 years ago and continues yet. The Naval Research Lab (NRL) was funded for six years starting in 1996. MITE2 was built after several changes which had a chord of 24.5 cm, and an aspect ratio of 1.45. This model was a rectangular fixed wing. Although the climb and maneuver performances of MITE2 was limited, it was an inherently stable flyer. The airspeed was 4-8 m/s. Other changes were implied to improve characteristics and so MITE3, MITE4, MITE5, and MITE6 were constructed [2]. Grasmeyer, J.M., and Keennon, M. T., presented black widow MAV that is one of the smallest and most successful MAV systems [2]. P. K. Burdman et.al. studied three types of MAVs, a conventional model, a sweptback flying wing and a squared flying wing, and then for ease and robustness reasons the last model was chosen[3]. H. L. Reed computationally investigated the effect of winglets to improve aerodynamic performance of tiny wings [4]. W. E. Green and P. Y. Oh described an additional flight modality enabling fixed-wing MAVs to supplement existing endurance superiority with hovering capabilities [5].

A. Sanna and B. Pralio used UAV to simulate an innovative piloting tool. UAVs allow to perform a lot of tasks such as surveillance, environmental monitoring, traffic control, and so on [6]. N. J. Farsaris et. al. mounted a camera on UAVs and applied airborne video transmission to a surface station in real time[7]. K. Altenburg made use of a team of UAVs and their research application concerned the management of military missions that utilize intelligent munitions that are capable of searching, detecting, identifying, and attacking targets in a battlefield [8].

In this paper we want to design a bodyless model aircraft or a flying wing UAV. To achieve this end a delta wing is presented and the effect of wing lets in aircraft stability is examined. The designed aircraft must carry a camera, and several sensors.

II. AIRCRAFT DESIGN

A. Conventional MAVs analysis

Aerodynamic analysis is one of the most helpful methods in the process of designing Micro Aerial Vehicle (MAV). No doubt, having a good anticipation of fluid flow around the MAV provides us with integral materials to design a MAV that produces sufficient lift & thrust.

Conventional airplanes have wings and engines to produce lift and thrust.

Manuscript received June 15, 2007; Revised November 17, 2007.

S. Afshar, M.SC. student, Advanced Dynamic and Control Systems Laboratory (ADCSL), Faculty of Mechanical Engineering, College of Engineering, University of Tehran, Tehran, Iran phone: 0098-912 379 13 76; fax: 0098-21-6111 48 13; E-mail: afshar_space@yahoo.com

A. Yousefi-Koma., PhD, Assistant Professor, Director, Advanced Dynamic and Control Systems Laboratory, University of Tehran, Faculty of Mechanical Engineering, College of Engineering, University of Tehran, Tehran, Iran. E-mail: aykoma@ut.ac.ir

H. Shahi, M.SC. student, Advanced Dynamic and Control Systems Laboratory (ADCSL), Faculty of Mechanical Engineering, College of Engineering, University of Tehran, Tehran, Iran phone: 0098-912 379 13 76; fax: 0098-21-6111 48 13; Email: hossein.shahi@gmail.com

D. Mohammadshahi, M.SC. student, Advanced Dynamic and Control Systems Laboratory (ADCSL), Faculty of Mechanical Engineering, College of Engineering, University of Tehran, Tehran, Iran phone: 0098-912 379 13 76; fax: 0098-21-6111 48 13; Email: dmohammadshahi@yahoo.com.

These two force components vary with different parameters such as the MAV's wing airfoil shape, size, angle of attack, and fabricating materials. This is one of the complexities of MAVs; since their lift and thrust vary to a large extent. Consequently stability, control, and navigation of these fascinating small creations are challenging.

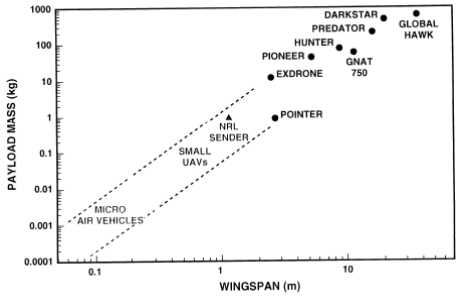

Fig 1:UAV wing span vs. payload

A-1) Flow Region

In order to make a precise simulation, It is material to demonstrate the flow region around micro aerial vehicle. MAVs operate in a low Reynolds number flight regime, in that speed and dimension of MAVs are small as it is shown in fig. 2.

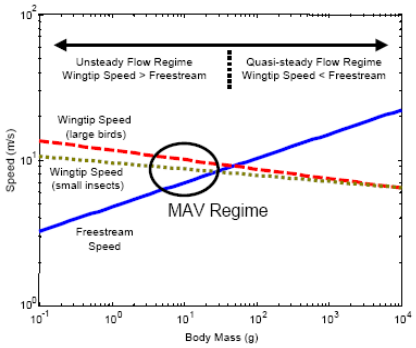

Fig. 2 Size of different flyers

The Reynolds number is a common ratio of inertial to viscous forces in aerodynamics, and is defined by Equation 1.

$$\mathrm{Re} = \frac{Inertia}{Viscous} = \frac{\rho S V^2}{\mu S V / l} = \frac{\rho l V}{\mu} \qquad (1)$$

where ρ is the fluid density, l is a characteristic length, V is the fluid velocity, and μ is the dynamic viscosity of the fluid.

While full-scale aircraft generally have Reynolds numbers greater than 1,000,000,

MAV Reynolds numbers will be less than 100,000. At low Reynolds numbers, the flow environment is laminar and highly viscous. This means that vortices are more difficult to sustain and that velocity gradients are very gentle unless large forces are applied. Because of this viscous flow environment, streamlined shapes such as airfoils are increasingly enveloped in a thick boundary layer, inhibiting their ability to generate lift. Due to greater skin friction, the profile drag increases. Consequently, the lift-to-drag ratios (L/D) of airfoils at low Reynolds numbers drop significantly.

A-2) Modeling of Moving Boundary

In case of existing moving boundaries, the solving region is not a constant volume any more. Since the shape of the model varies during time, the grid network should be changed at every moment of solution time. There are various methods to model moving boundaries. Here two of them are discussed.

1. Smoothing Method
2. Remeshing Method

A-3) Smoothing Method

In this method, elements are supposed as connected springs that are free at initial state. Boundary movement causes tension/ compression forces in springs that are proportional to displacement in spring direction.

Fig. 3 shows two views of a cylinder before and after boundary movement that is modeled by smoothing method.

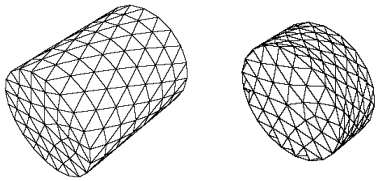

(a) (b)

Fig. 3 Cylinder view a)before the boundary Movement. b) after boundary movement

A-4) Remeshing Method

In region with triangular and pyramidal elements, remeshing method is usually applied. When the boundary movement is much larger than element size, mesh grid might damage. In order to prevent following inconveniences, destroyed elements are replaced with new elements by remeshing the critical regions.

A-5) Modeling Steps

The modeling process consists of three steps:

1. Modeling the geometry
2. Meshing
3. Simulation of flight

A-6) Modeling the geometry

It is enough to simulate only half of the MAV's body in FLUENT, in that the 3D model is axisymmetric. The wing model is imported from Solidwork to the Gambit. This step is followed by defining the solution limits. It should be taken into accounts that too small solution limits result in making big errors, whereas too large solution limits require extensive solving time. Hence it is very important to choose proper solution limits.

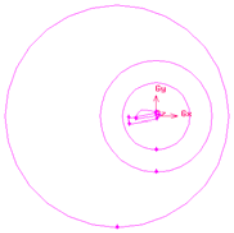

Fig. 4 Dividing the solution region into three parts

A-7) Meshing

It is essential to create fine elements near solid model. Besides, these elements should be analogous. Otherwise errors might become significant in dynamic mesh solution. On the other hand the upper limit of element numbers is limited by solving time. Consequently solution region is divided into three parts as it is shown in fig. 4. The first region contains fine elements near the body and the other two regions contain coarse elements. Fig. 5 shows meshing of the whole solving region.

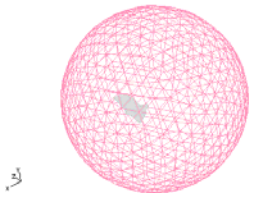

Fig. 5 Meshing the whole solving region

A-8) Simulation of flight

Simulation of flight gives us a good perspective of meshing and fluid flow around MAV.

Fig. 6 shows the pressure distribution around MAV wings. The aerodynamic forces are due to positive and negative pressure gradients that are shown in pressure contours in fig 6.

As fig. 6 shows the MAV body pulls the streamline toward and lessen the mean of pressure under wing. However it pushes the flow stream and increases the mean pressure on the wing. Decreasing the pressure difference of two wing sides leads to a decrease in lift at wing root and consequently a decrease in lift to drag ratio. Replacing body with airfoil sections makes the lift force to increase whereas the drag force decrease.

B. Bodyless aircraft design

The first step in plane designing is to determine wing area. This part of designing plays an important roll in payload endurance threshold. On the other hand wing must cover all parts of the air craft. According to the model weight, wing span and loading value are selected. The wing area can be calculated using equation (2):

$$S = W / (W/S) \qquad (2)$$

in the above equation S is the wing area.

Model aspect ratio is a function of wing shape. A delta shape wing is the proper selection to cancel the plane fuselage in this manner that the separating space between fuselage and wings ca be replaced by wing sections. Delta wing aspect ratio is low and set equals to 4 for this model. The wing span may be determined using the equation (3):

$$b = \sqrt{AR \times S} \qquad (3)$$

The delta wing operation is different from other conventional rectangular wings. The air flow is divided into two components on the leading edge. One component is perpendicular to the leading edge and the other component is parallel to this edge. Only the first component is essential in lift generating, while the parallel component produces drag force. Therefore in these wings lift to drag ratio is lower than other wings. Flying wings do not have conventional vertical and horizontal tail. In order to secure the stability requirements the wing has backward sweep, negative twist, and dihedral. To compensate longitudinal stability reflex sections are used. Elevons are used to this end. Also to increase roll and yaw stability two winglets are added to the wing tips. This wing shape selection affects all other behavior of plane.

Wing shape and span influence lift distribution along the wing span. Lift distribution is shown for some wings in fig. 7 [15]. Lift distribution have an important effect on drag force. Tapering the wing make the behavior of wing close to elliptical wing and aerodynamic efficiency may become near 1. The wing may be divided in two sections: central section that occupy 40% of wing and covers the equipments of plane, and the other part produce the main lift force.

Base lift distribution (distribution of lift along wing span when total lift is zero) and added lift distribution must be determined [14]. It is needed to calculate lift distribution at

a **b**

Fig 6: Pressure contour a) on the wing, b) under wing

any angle of attack. Here it makes use of fig. 7. Total lift can be determined using equation (4):

$$C_{li} = a_i .(\alpha - \alpha_0 - \varepsilon)$$
$$C_L = \int_0^{b/2} a_i .(\alpha - \alpha_0 - \varepsilon).C. \; dy \Big/ \int_0^{b/2} C.\, dy \qquad (4)$$

In the above equation a_i is the lift curve slop and ε is the induced angle of attack. When total lift is zero then there is no induced angle of attack and total lift can be calculated from equation bellow:

$$C_L = \frac{1}{S}\left(\sum_{i=1}^{n} a_i \times (\alpha - \alpha_{oi} + \alpha_i') \times C_i \times b_i\right) \qquad (5)$$

In the above equation a_i is the slop of lift vs. angle of attack curve (linear section), α_i' is the angle of attack in each section due to its chord configuration with respect to central chord, b_i is the length of each wing section (wing sections are variable from central axis to wing tip.) C_i is section chord length, and α_{i0} is the zero lift angle of attack. After several trials and errors it is usually possible to find zero lift angle of attack. The results are shown in table 1, 2, 3.

α_i' can be achieved from configuration of wing sections and the angle of the elevon. Fig 8 shows leading edge and trailing edge in the front view of wing. Furthermore, each wing section deflection and the position of elevon with respect to section chord line is shown in fig. 9.

Geometric angle of attack α_i' can be obtained from equation (6):

$$\alpha_i' = \gamma_i + \tan^{-1}\frac{h_i}{C_i} \qquad (6)$$

Supposing that all a_i s are the same [14], the value of α_o can be calculated using equation (7):

$$C_L = \frac{\sum b_i.C_i.C_{li}}{S} = \frac{2\times\int_0^{b/2} C.C_l\, dy}{S} \qquad (7)$$

A method is required to determine lift distribution at any angle of attack. One method is to make use of C_l/C_L. An example of this distribution presents in fig. 7. Considering a_i s is constant, the equation (7) can be written in the form of equation (8):

$$b_0 = \frac{(\alpha - \alpha_0 - \varepsilon)\int_0^{b/2} C.dy}{\int (\alpha - \alpha_0).C.dy - \int \varepsilon.C.dy} \qquad (8)$$

In the above equation b_0 is the C_l/C_L value in each point of the lift distribution diagram, and α_0 is the mean zero angle of attack. Equation (8) may be simplified to:

$$b_0 = \frac{(\alpha - \alpha_0 - \varepsilon).C.b/2}{(\alpha - \alpha_0).C.b/2 - C\int \varepsilon.dy} \qquad (9)$$

Supposing $Z = \int \varepsilon.dy$, it can be written as equation (10):

$$b_0.Z - b/2.\frac{dZ}{dy} = (b_0 - 1).(\alpha - \alpha_0).b/2$$
$$at \quad y = b/2 \qquad \varepsilon = \alpha - \alpha_0 \qquad (10)$$

If C_l/C_L is known for desired configuration curve, equation (10) can be used to calculate lift distribution for any wing sections.

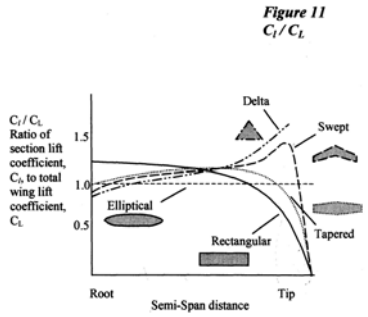

Fig 7: Lift distribution along wing span for some wings.

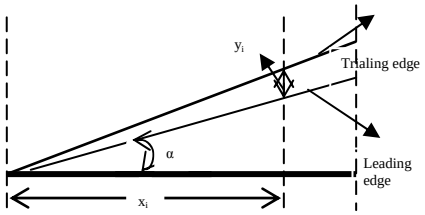

Fig 8: The front view of wing.

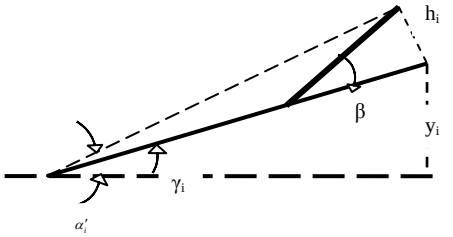

Fig 9: A schematic of wing section deflection.

In the first step of designing the model, it is supposed that lift distribution is ideal. Then some cautions are preserved. Wing sections are different from root to tip. Also the elevon

length is variable. As was mentioned before to conserve longitudinal stability, reflex airfoil is used instead of horizontal tail. Reflex sections produce downward forces when the elevon angle is positive (fig. 10). Consequently longitudinal stability is improved. This effect is more at wing tips , since the distance from tips to center of gravity is more long. So elevon length is to be increased.

Now it is possible to evaluate mean aerodynamic center. This position can be obtained from equation bellow:

$$\bar{X} = \frac{2\int_0^{b/2} C_{la}.C.x.dy}{C_L.S} \qquad (11)$$

where C_{la} is the lift distribution, C is each section chord line length, x is the distance between point located at the ¼ chord length and line which is placed in horizontal plane and is perpendicular to the central chord at nose point, y is each section distance from central chord, C_L is total lift force, S is the wing area, and $\bar{X}$ is the mean aerodynamic center.

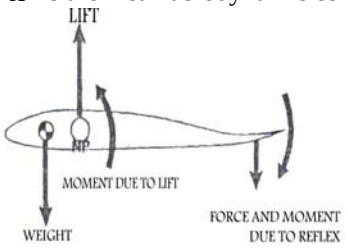

Fig. 10 The schematic of reflex section.

Also total pith moment coefficient around aerodynamic center can be found from the following equation:

$$C_{Mac} = \frac{-\int_0^{b/2} C_{lb}.C.x.dy + \int_0^{b/2} C_{mac}.x.C^2.dy}{\int_0^{b/2} C^2.dy} \qquad (12)$$

In this equation C_{lb} is added lift distribution, C_{mac} is the pith moment of each section around aerodynamic center, and C_{Mac} Also total pith moment coefficient around aerodynamic center [14]. Aerodynamic chord is defined as follow:

$$\bar{\bar{C}} = \frac{2\times\int_0^{b/2} C^2.dy}{S} \qquad (13)$$

$\bar{\bar{C}}$ is the aerodynamic chord. This definition is used for longitudinal stability computations.

To compensate longitudinal stability a parameter that is named as Margin static is defined. The stability is reliant on the $-dC_{M.G}/dC_L$ value. More positive value leads to further stability. In this condition model is said to have positive Margin static. Stability equation can be indicated as bellow:

$$-\frac{dC_{MG}}{dC_L} = \frac{(Ho - H)}{\bar{\bar{C}}} \qquad (14)$$

In this equation Ho is the aerodynamic center, and H is the center of mass.

As was stated before wing sections are different from root to tip. To select proper sections ease of construction, and correct aerodynamic behaviors should be considered [11,13]. Designfoil simulator software is used to this end. Lower face of all sections is selected to be flat in order to provide ease of assembly.

III. Aerodynamic properties

A. General properties

Savita2 is designed to have no fuselage; therefore it may have some different aerodynamic properties. This model is a radio control electronic model. Its instruments are as follow: A brushless dc motor with power of 60wat, three servo motors, a 400mAh two cell Nicad battery, a six channel receiver, a motor speed control, and a camera is mounted to the model. Total mass of model is about 270gr. Wing span is 85 cm, sweep angle is 30^0, dihedral is about 2^0 , and also there is a negative twist angle equals 2^0.

As was cited before the wing divided to two sections first section cover electronic instruments. Taper ratio of this section is supposed to be 0.7. The second section taper ratio is determined as 0.75

B. Stability Analysis

Model wing semi span is divided to five parts, constructed from 6 sections. Stability properties are determined using ideal lift distribution.

If the angle of elevon is positive 4^0 (upward) then aerodynamic properties are as follow:

Lift coefficient (C_L)	0.2
Zero angle of attack (α_0)	-0.2^0
Mean aerodynamic center ($\bar{X}$)	16.84
Pith moment coefficient around aerodynamic center (C_{Mac})	0.036
Mean aerodynamic chord ($\bar{\bar{C}}$)	28.4
Center of gravity (C.G)	10.4
Margin static	26%

Also for angle of elevon positive 2^0, aerodynamic properties are calculated in the same way:

Lift coefficient (C_L)	0.3
Mean aerodynamic center ($\bar{X}$)	17
Pith moment coefficient around	0.019

Aerodynamic center (C_{Mac})	
Center of gravity (C.G)	15.4
Margin static	6.5%

For the first configuration, model has further stability but less maneuverability. Also total lift coefficient is low. On the other hand for the second configuration longitudinal stability is relatively less but the model has more maneuverability. Also because of tip vortexes actual lift force is less than computed value. So C.G. is more farther from leading edge than its ideal situation and the elevon angle assume to be closer to positive 2^0.

Model maximum speed is determined from equation bellow [12]:

$$(U_\infty)_{max} = \frac{2 \times P_{req}}{C_D \times \rho \times S} = 19.4 \qquad (15)$$

To preserve roll and yaw stability, two 30^0 winglets with are added to wing tips in the second model.

IV. Simulation and Test

A. Model construction

To construct the model and also maintaining low weight, balsa wood is used. Here a 2D plot of Savita2 is shown in fig. 11.

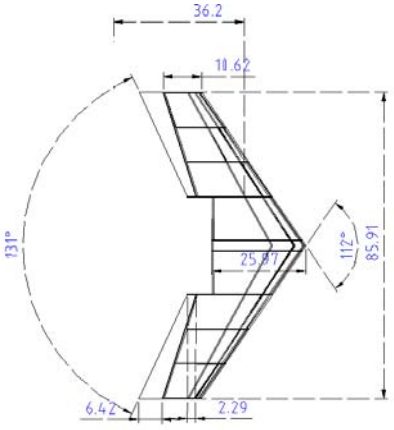

Fig. 11 2D plot of Savita2.

Firstly the model frame is built. To construct the model frame, airfoil sections are cut from balsa wood and these sections configure overall shape of the plane and then it is covered to complete the model (fig. 13). Electronic instruments are mounted in the central part of the wing (fig 12). The model has two servo motors that are connected to elevons. This model is a radio control model.

B. Model test

Final test was done after covering the model. In the second step, camera was mounted on Savita2 and flying test was done. It seems that the model has a good accordance with the theoretical computations. Another model was constructed in which winglets were removed (Savita2.1) and flying test was done again. Fig. 14 shows a schematic of Satita2 flying test.

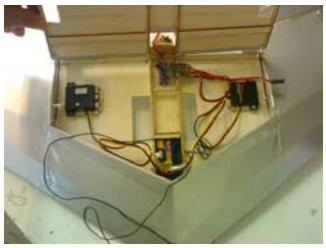

Fig. 12 A schematic of model instrument mountening.

Fig. 13 An isometric view of covered Savita2.

Fig. 14 A schematic of flying test of Savita2.

C. Test results

Results of tests are as follow: in the first test, model showed good maneuverability and acceptable stability. Maximum speed was about 15m/s, and flying time was 35min. In the second test, the maximum speed was about 14m/s and flying time was 25 minutes. The MAV showed a better stability with proper maneuverability

V. Conclusion

The goal was to design a Micro Aerial Vehicle without any fuselage conserving stability properties of conventional aircrafts. Consequently, two delta shape wing models were fabricated, one model with winglets and the other one without winglets. To compute aerodynamic properties it is assumed that lift distribution is ideal.

Flight tests indicated stability properties become poor when winglets omitted. It may be due to the ideal lift distribution assumption. Adding winglets declines tip vortex effect and bring actual and ideal wing behavior close together.

Moreover, it is observed experimentally that winglets can increase roll and yaw.

REFERENCES

[1] T. J. Mueller, Fixed and flapping wing aerodynamic for Micro-Air-Vehicle application, vol. 195, AIAA,2000.
[2] T. J. Mueller, J. C. Kellogg, P. G. Ifju, S. V. Shkarayev, Introduction to design of fixed-wing MAV,
[3] B. K. Burdman, M. Guest, F. Nieto, F. Pradeloux, J. Senabre, Design of micro air vehicle (MAV), Linkoving ut., institute of technology, 2004
[4] H. L. Reed, K. D. Squires, W. S. Saric, On the effect of winglets on the performance of Micro-Aerial-Vehicles, ASU symposium on research in engineering and applied sciences, 2003
[5] W. E. Green, P. Y. Oh, A MAV that flies like an airplane and hovers like a helicopter, IEEE/ASME, 2005, pp693-697
[6] A. Sanna, B. Pralio, An Innovative Tool for Simulating and Controlling Mini Air Vehicles, WSEAS Transactions on Information Science and Applications, 2005.
[7] N. J. Farsaris, T. D. Xenos, P. P. Stavroulakis, Airborne Video Transmission for Naval and Coast Guard Applications, 6th WSEAS Int. Conf. on Electronics, Hardware, Wireless and Optical Communications, 2007.
[8] K. Altenburg, J. Schlecht, K. E. Nygard, An Agent-based Simulation for Modeling Intelligent Munitions, 2th WSEAS Int. Conf. on Simulation, Modeling and Optimization, 2002.
[9] Th. Rakotomamonjy, Th. Le Moing, Mr. Ouladsine. Simulation Model of a Flapping-wing Micro Air Vehicle, EMAV 2004, Braunschweig, Germany, July 2004
[10] S. Ho, H. Nassef, T.N. Pornsinsirirak and Y.C. Tai, Unsteady aerodynamics and flow control for flapping wing flyers, Prog. Aerosp. Sci. 39 (2003), pp. 635–681.
[11] J. J. Bertin, M. L. Smith, Aerodynamic for engineers, Prentice Hall, 2002.
[12] H. L. Chevalier, Model airplane design and performance for the modelers, Texas A&M University, 1993.
[13] Ira H. Abbott, A. E. Von Doenhoff, theory of wing section,
[14] F. G. Irving, An Introduction to the Longitudinal Static Stability of Low-Speed Aircraft, Pergamon Press, Oxford, UK, 1966.
[15] R.H. Barnard, D.R. Philpott, Aircraft flight, Pearson Education, 2003.

Aghil Yousefi-Koma, PhD, was born in 1963 in Fouman, Iran. Dr. Yousefi-Koma got his PhD from Carleton University, Aerospace Engineering in 1997 and his MSc and BSc from University of Tehran, Mechanical Engineering in 1989 and 1986 respectively. He has been an assistant professor at the Faculty of Mechanical Engineering in University of Tehran since 2005. He is also serving as the director of University of Tehran Technology Incubator, the director of the Advanced Dynamic and Control Systems Laboratory (ADCSL), and the director of Centre for Advanced Vehicles (CAV). Dr. Yousefi-Koma's main field of interest includes system dynamics, control, smart structures, micro-robotics, micro-underwater vehicles, and micro-aerial vehicles. He is the author of more than 100 refereed journal and conference papers and technical reports. He is also a co-author of the "Intelligent Materials" book by The Royal Society of Chemistry, 2008. Before joining University of Tehran Dr. Yousefi-Koma had been working in the Institute for Aerospace Research of National Research Council Canada (NRC), SNECMA Motors, and Canadian Space Agency (CSA) between 1997-2005.

D. Mohammadshahi (M'08) was born in Iran on may, 5, 1983. Donya is a M.Sc. student in Mechanical Engineering, in Advanced Dynamics and Control Systems Laboratory (ADCSL), Faculty of Mechanical Engineering, College of Engineering, University of Tehran, Tehran. Iran. She works under supervision of Dr. Aghil Yousefi-Koma, Assistant Professor at School of Mechanical Engineering, University of Tehran. In 2005, she received the B.Sc. degree in Mechanical Engineering from the University of Tehran.

She has been the **Deputy Director of Advanced Dynamics and Control Systems Laboratory (ADCSL)**, Faculty of Mechanical Engineering, College of Engineering, University of Tehran, Tehran. Iran, since Jan, 2007. Her previous work experiences are 1st: **Project Manager** of the funded industrial project, "Design, Fabrication and Control of a Biomimetic Underwater Vehicle (BUV)". 2nd: **Project Manager** of the funded Research project, "Robotic and Mechatronics Master Plan". 3rd: **Member of the Design Group** in the industrial/research project, "Design, Fabrication and Analysis of a Micro Underwater Vehicle (MUV)". 4th: **Member of the Analysis Group** in the industrial/research project, "Design, Fabrication and Analysis of a Flapping Wing Micro Aerial Vehicle (MAV)", 5th: A learner at research and development center of Iran Khodro Co., and 6th: A team member in Analysis of different structures of beams using finite element method with ADAMS and ANSYS as an research project. Her research interests are in the fields of Advanced Micro Vehicles, Experimental Mechanics, Robotics and Artificial Intelligence, Engineering Rheology, and Fluid Mechanics (Computational).

Hossein Shahi was born in 1983 in Tehran, Iran. He is now a MSc. student of Mechanical Engineering at Tehran University and got his BSc. from University of Tehran, Mechanical Engineering in 2006. He has been a research assistant in Advanced Dynamic and Control Systems Laboratory since 2006. His main research interests and experience include control, system identification, smart material and micro-aerial vehicles.

.

Table 1: Airfoil sections data for elevon 40 positive angle.

Number of sections	**Zero lift angle of attack α_0**	**Lift coefficient Cl**	**Drag oefficient Cd**	**Pith moment coefficient Cm**
1	-3.8	0.429	0.007	-0.0692
2	-2.35	0.273	0.0069	-0.0274
3	-1.3	0.085	0.0071	-0.0036
4	-0.24	-0.109	0.0076	0.0175
5	1.12	-0.333	0.0081	0.034

Table 2: Airfoil sections data for elevon 30 positive angle.

Number of sections	**Zero lift angle of attack α_0**	**Lift coefficient Cl**	**Drag oefficient Cd**	**Pith moment coefficient Cm**
1	-3.8	0.429	0.007	-0.0692
2	-2.8	0.325	0.0071	-0.0386
3	-1.8	0.149	0.007	-0.0161
4	-0.89	-0.035	0.0075	0.0052
5	0.42	-0.261	0.0079	0.0257

Table 3: Airfoil sections data for elevon 20 positive angle.

Number of sections	**Zero lift angle of attack α_0**	**Lift coefficient Cl**	**Drag oefficient Cd**	**Pith moment coefficient Cm**
1	-3.8	0.429	0.007	-0.0692
2	-3.25	0.377	0.0071	-0.0497
3	-2.4	0.214	0.0071	-0.0286
4	-1.55	0.039	0.0075	-0.007
5	-0.27	-0.189	0.0077	0.0172